Proceeding of the 13th National Mechanical Engineering Conference
2-3 December 1999, Royal Cliff Beach Resort Hotel, South Pattaya, Cholburi

Simulation of Turbulent Flow through a Circular Orifice

Pongjet Promvonge
Department of Mechanical Engineering, Faculty of Engineering,
King Mongkut's Institute of Technology Ladkrabang, Bangkok 10520, Thailand.
Email: kppongje@kmitl.ac.th

and

Kulthorn Silapabanleng
Department of Mechanical Engineering, Faculty of Engineering,
Chulalongkorn University, Bangkok 10330, Thailand.

Abstract

The paper presents a numerical simulation of a steady turbulent airflow in a circular duct containing an orifice plate. A Finite Volume approach with a non-uniform and staggered grid system is employed in the present simulation. To account for the turbulence nature of the flow, the standard k-ε turbulence model is incorporated in the time-averaged governing equations. Effects of numerical diffusion on the calculated results are also investigated by comparing between a second-order-differencing scheme for the convection transport and the first-order hybrid scheme. The calculated solutions are in close agreement with 3D LDA measurements. The computations of the flow reveal that the use of a second-order scheme leads to more accurate results than that of a first-order scheme.

1. Introduction

The orifice meter is a device commonly used for measuring fluid flow in industrial processes such as metering flow in the natural gas industry. Although more accurate metering methods are available, the orifice plate continues to be preferred. The popularity of the orifice meter can be attributed primarily to its simplicity, relatively low cost and little maintenance requirements in comparison with other fluid meters. The orifice plate becomes the essential part of a fluid flow meter when installed in a pipe such that the fluid stream must negotiate the constriction.

By far the most common orifice plate installation is that of the concentric round orifice plate. In this type of arrangement the orifice is round and the plate is mounted between pipe flanges. The plate is positioned perpendicular to a fully developed pipe flow while at the same time the circular orifice is concentric with respect to the (circular) pipe interior. Other types of orifice plate exist, such as square orifices, series and non-concentric. Also, the inner edge of the orifice is machined in one of several different ways. Some orifice plates are square edged while others are rounded and beveled. This study is concerned with the concentric, round, beveled orifice plate.

Most of the work thus far on orifice meters has focused almost entirely on the determination of discharge coefficients. There have been a handful of attempts to study in detail the flow field in the vicinity of the orifice plate. It is believed that knowledge concerning details of the orifice flow field will lead the way to improvements in metering accuracy. These improvements could come via improved determination and prediction of discharge coefficients.

This paper deals with the simulation of turbulent flow through an orifice plate with a view to increasing the knowledge of orifice meter flow. The mathematical model including the k-ε turbulence model, numerical solution and other computational details is described. Comparisons of the calculated gas axial velocity with 3D LDV measured data [4] are made to evaluate the turbulence models and the numerical schemes used.

2. Mathematical Modelling

2.1 Governing Equations and Closures

For constant density, isothermal turbulent flows, the time-averaged incompressible Navier-Stokes equations in the Cartesian tensor notation can be written in the following form:

$$\frac{\partial}{\partial x_i}(\rho u_i) = 0 \tag{1}$$

$$\frac{\partial(\rho u_i u_j)}{\partial x_j} = -\frac{\partial p}{\partial x_i} + \frac{\partial}{\partial x_j}(\bar{t}_{ij} + \tau_{ij}) \tag{2}$$

The mean viscous stress tensor is approximated as:

$$\bar{t}_{ij} = \mu\left(\frac{\partial u_i}{\partial x_j} + \frac{\partial u_j}{\partial x_i}\right) \tag{3}$$

where μ is laminar viscosity. Due to the nonlinearity of equation (2), the averaging process employed introduces the unknown correlation the time-averaged Reynolds stress tensor, τ_{ij} ($= -\rho\overline{u_i' u_j'}$) that are obtained from

turbulence models [1, 2, 3, 10]. In the present study, the standard k-ε turbulence model [1, 10] is adopted and the Reynolds stress is linearly related to the mean rate of strain by a scalar eddy viscosity. The standard version relates the turbulent eddy viscosity to the turbulence kinetic energy k and the dissipation rate ε through Boussinesq's approximation [8] as:

$$\tau_{ij} = -\frac{2}{3}\delta_{ij}(\rho k) + \mu_t\left(\frac{\partial u_i}{\partial x_j} + \frac{\partial u_j}{\partial x_i}\right) \quad (4)$$

where μ_t is the turbulent eddy viscosity. In the k-ε model the turbulent viscosity is related to k and ε by

$$\mu_t = C_\mu \rho \frac{k^2}{\varepsilon} \quad (5)$$

The two turbulence quantities in equation (5), k and ε, are obtained from the following transport equations which are solved simultaneously with governing equations (1) and (2):

$$\frac{\partial}{\partial x_j}(\rho u_j k) = \frac{\partial}{\partial x_j}\left(\frac{\mu_e}{\sigma_k}\frac{\partial k}{\partial x_j}\right) + \widetilde{G} - \rho\varepsilon \quad (6)$$

$$\frac{\partial}{\partial x_j}(\rho u_j \varepsilon) = \frac{\partial}{\partial x_j}\left(\frac{\mu_e}{\sigma_\varepsilon}\frac{\partial \varepsilon}{\partial x_j}\right) + \frac{\varepsilon}{k}(C_{\varepsilon 1}G - C_{\varepsilon 2}\rho\varepsilon) \quad (7)$$

in which G represents the rate of generation of turbulent kinetic energy while $\rho\varepsilon$ is its destruction rate. G is given by:

$$G = \mu_t\left[\left(\frac{\partial u_i}{\partial x_j} + \frac{\partial u_j}{\partial x_i}\right)\frac{\partial u_i}{\partial x_j}\right] \quad (8)$$

The boundary values for the turbulent quantities near the wall are specified with the wall function method [6]. The empirical constants C_μ, $C_{\varepsilon 1}$, $C_{\varepsilon 2}$, σ_k, and σ_ε in the turbulent transport equations are assumed to have the values of 0.09, 1.44, 1.92, 1.0 and 1.3 [8, 10] respectively.

2.2 Common Form for the Equations

All the governing partial differential equations can be re-organised and expressed in a standard form that includes the convection, diffusion, and source terms [5, 9] for 2-D axisymmetric flows as follows:

$$\frac{\partial}{\partial x}(\bar{\rho}u\phi) + \frac{1}{r}\frac{\partial}{\partial r}(r\bar{\rho}v\phi) - \frac{\partial}{\partial x}\left(\Gamma_{\phi x}\frac{\partial \phi}{\partial x}\right) - \frac{1}{r}\frac{\partial}{\partial r}\left(r\Gamma_{\phi r}\frac{\partial \phi}{\partial r}\right) = S_\phi \quad (8)$$

where ϕ may stand for any variable including the velocity components, $\Gamma_{\phi x}$ and $\Gamma_{\phi r}$ are the exchange coefficients for ϕ, and S_ϕ is the source term.

Detailed expressions of $\Gamma_{\phi x}$, $\Gamma_{\phi r}$ and S_ϕ for different ϕ's are summarised in Table 1 below.

Nomenclature

$C_{\varepsilon 1}$, $C_{\varepsilon 2}$	constants in the dissipation rate equation
C	convection term
C_μ	constant in the k-ε turbulence model
D	diffusion term; dimension
D	pipe or duct diameter
d	orifice diameter
G	stress generation
k	turbulence kinetic energy
l	turbulence characteristic length scale
p	mean pressure
p_{in}	inlet wall pressure
p_{out}	outlet wall pressure
r	radial co-ordinate; radius
R	pipe radius
Re_D	Reynolds number based on pipe diameter
S	general source term; swirl number
t_{ij}	viscous stress tensor
u_i'	fluctuating velocities in direction x_i
$\overline{\rho u_i' u_j'}$	Reynolds stresses
u	time-averaged velocity in x-direction
v	time-averaged velocity in r-direction
x	axial co-ordinate

Greek Symbols

δ_{ij}	Kronecker delta tensor
ε,	dissipation
ϕ	generalised dependent variable
Γ_ϕ	exchange coefficient
β	ratio of pipe to orifice diameter (d/D)
μ, μ_t	dynamic viscosity, eddy-viscosity
μ_e	effective viscosity, $(=\mu_t + \mu)$
ρ	density
σ_ϕ	Schmidt or Prandtl numbers for the scalar ϕ
τ_{ij}	Reynolds stress tensor

Subscripts

e	effective
t	turbulence
i, j, k	Cartesian indices

Superscripts and Overbars

′	fluctuating quantity in time-averaging
—	mean quantity

Table 1 Summary of the governing equations.

Conservation of	ϕ	$\Gamma_{\phi x}$	$\Gamma_{\phi r}$	S_ϕ
Mass	1	0	0	0
x-momentum	u	μ_e	μ_e	$\frac{\partial}{\partial x}\left(\mu_e \frac{\partial \tilde{u}}{\partial x}\right)+\frac{\partial}{r\partial r}\left(r\mu_e \frac{\partial \tilde{v}}{\partial x}\right)-\frac{\partial}{\partial x}\left(\bar{p}+\frac{2}{3}\bar{\rho}k\right)$
r-momentum	v	μ_e	μ_e	$\frac{\partial}{\partial x}\left(\mu_e \frac{\partial \tilde{u}}{\partial r}\right)+\frac{\partial}{r\partial r}\left(r\mu_e \frac{\partial \tilde{v}}{\partial r}\right)-\frac{\partial}{\partial r}\left(\bar{p}+\frac{2}{3}\bar{\rho}k\right)-\frac{2\mu_e \tilde{v}}{r^2}$
Turbulent kinetic energy	k	μ_e/σ_k	μ_e/σ_k	$G-\rho\varepsilon$
TKE dissipation rate	ε	μ_e/σ_ε	μ_e/σ_ε	$(C_{\varepsilon 1}G-C_{\varepsilon 2}\rho\varepsilon)\frac{\varepsilon}{k}$

where $\sigma_k = 1.0$, $\sigma_\varepsilon = 1.3$, $C_{\varepsilon 1} = 1.44$, $C_{\varepsilon 2} = 1.92$, $\mu_e = \mu_t + \mu$, $G_k = \mu_e\left\{2\left[\left(\frac{\partial \tilde{u}}{\partial x}\right)^2+\left(\frac{\partial \tilde{v}}{\partial r}\right)^2+\left(\frac{\tilde{v}}{r}\right)^2\right]+\left(\frac{\partial \tilde{v}}{\partial x}+\frac{\partial \tilde{u}}{\partial r}\right)^2\right\}$

2.3 Solution Procedure

In the present computation, the time-averaged Navier-Stokes equations, the TKE equation, and the TKE dissipation rate equation are solved numerically by a control-volume finite-difference method [5, 9] together with the the k-ε model, equation (4). All equations are in a generalised form of equation (8). The SIMPLE algorithm is utilised for pressure-velocity de-coupling and iteration [5, 8]. The hybrid [9] and the second order upwind (SOU) [7] schemes were used for discretising convection and diffusion transports on a staggered grid cell. The underrelaxation iterative TDMA line-by-line sweeping technique is used for solving the resultant finite-difference equations. The computation was carried out using a PC (Pentium III - 450 MHz) computer. About 5,000 iterations were needed to achieve satisfactory convergence for each calculation case, which requires about 15 minutes of computer time.

3. Flow through an Orifice of Nail [4]

A flow in pipe with a circular orifice of Nail [4] was employed in the present simulation. A schematic configuration of the duct orifice is shown in Fig. 1 below. The pipe with a length of 9D has a diameter of 25.4 mm and the 3.2-mm thick orifice diameter is 12.7 mm. Profile measurements of centerline axial velocities, wall-static pressure, Reynolds stresses, and wall shear stresses were measured by using Laser Doppler anemometer (LDA). The flow had the Reynolds number (Re) of 1.84×10^4 and rate of mass flow of 1.356×10^{-2} kg/s with temperature at 300K (see Table 2 below for specifications).

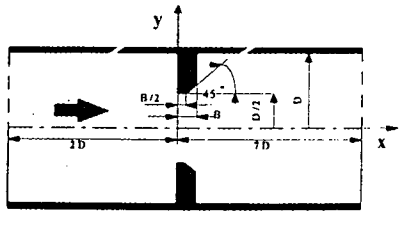

Fig. 1 Geometry of pipe with the orifice.

Table 2 Data for flow through an orifice plate [4].

Parameter	Magnitude
Test section characteristics	
Pipe diameter (D), *m*	0.0254
Orifice diameter (d), *m*	0.0127
pipe length (L), *m*	1.8
Inlet fluid properties (air)	
Mean axial velocity, *m/s*	5.6
Temperature, K	300
Reynolds number	1.84×10^4

4. Results and Discussion

The comparisons between the predicted results by the k-ε turbulence model with different numerical schemes and the measured data of the flow are presented in Figs. 2 through 7. The predicted gas pressure and centerline axial velocities are compared with the measurements, where solid or dash curves are represented for the calculated results while open circles for the measured data.

The computational results are based on a 70x30 non-uniform grid with refinement in the vicinity of the orifice. Grid independence of the numerical results was verified with a 90x50 finer grid. It is found that the differences for both the base grid and the finer grid in local flow properties are marginal. This suggests that grid independent solutions can be obtained with a 70x30 grid, which is used throughout the computations. In order to reduce uncertainties in the inlet profiles of the mean flow field, the inlet boundary conditions were specified at x/D = -2.0 for which measured data was available, apart from the radial velocity v which is set to zero.

The distributions of centerline axial velocity predicted with the hybrid and the SOU schemes are compared with the measured data in Fig. 2. A closer examination reveals that predictions with both the

schemes are in generally good agreement with the measurements. However, for prediction with the hybrid scheme, under-predicted results are seen in the orifice region in comparison with experimental data. The use of the SOU leads to substantial improvement for this flow.

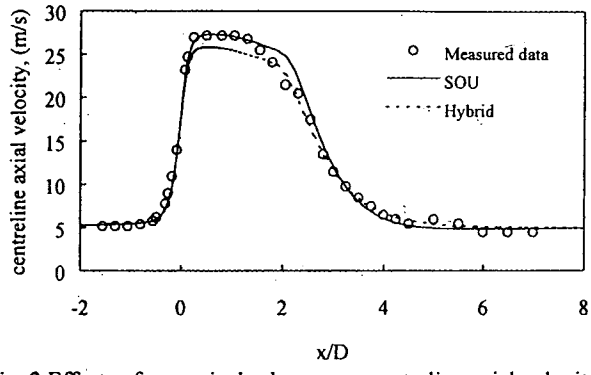

Fig. 2 Effects of numerical schemes on centerline axial velocity profiles with measurements.

Figure 3 compares the profiles of static pressure along the wall using the hybrid and the SOU schemes with the measurements. It is found that there is a high-pressure drop across the orifice. Predictions with both numerical schemes show favourable agreement in upstream region of the orifice. However, immediately after the orifice plate, the calculated wall pressure rises faster than the experiment shows. At downstream regions from the orifice, the SOU results mimic experimental data very well while the hybrid scheme ones are over-predicted. Again, the use of the SOU results in significant improvement for this flow

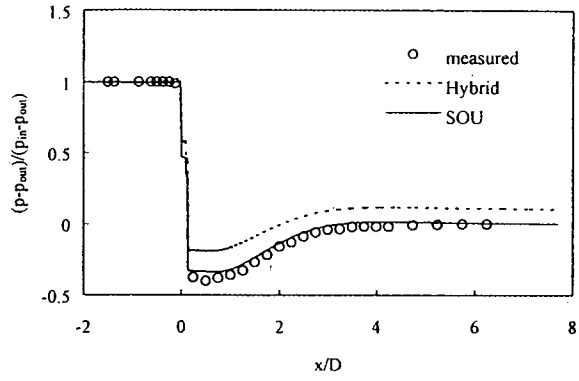

Fig. 3 Effects of numerical schemes on wall-static pressure profiles with measurements.

Streamlines predicted with the hybrid and SOU schemes are shown in Fig. 4 and Fig. 5 respectively. Two recirculation zones are found; one is at the corner upstream of the orifice and the other, a large recirculation zone, a downstream region one. The size of the recirculation zone calculated by the hybrid is slightly larger than that by the SOU. The center of recirculation predicted by the SOU is at about x/D = 1 and r/R = 0.7 while at about x/D = 0.85 and r/R = 0.7 is seen for the hybrid. The reattachment length, an important measure of the quality of numerical results, is well predicted ($x_{r,exp}$ = 2.25D, $x_{r,calc}$ = 2.23D for SOU, and $x_{r,calc}$ = 2.1D for hybrid).

Velocity vectors predicted by the hybrid and SOU schemes are depicted in Figs. 6 and 7 respectively. High velocities are observed in the core region in a range of x/D = 0 to 3 downstream of the orifice.

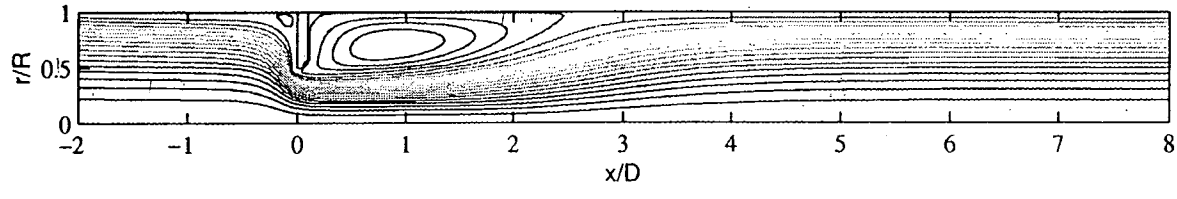

Fig. 4 Streamlines predicted by the hybrid scheme

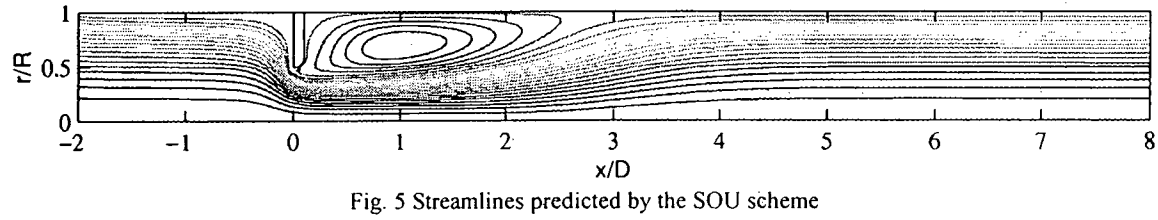

Fig. 5 Streamlines predicted by the SOU scheme

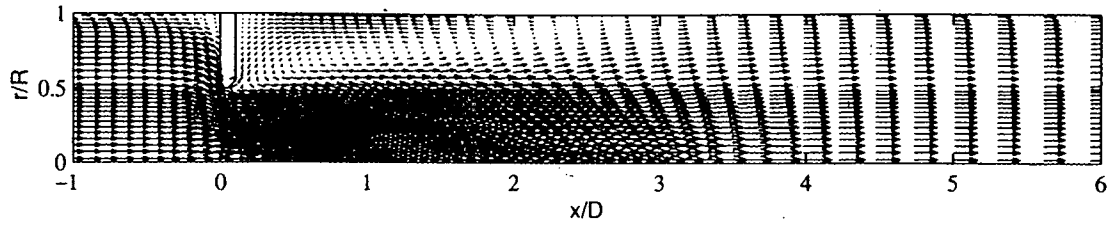

Fig. 6 Velocity vectors predicted by the hybrid scheme

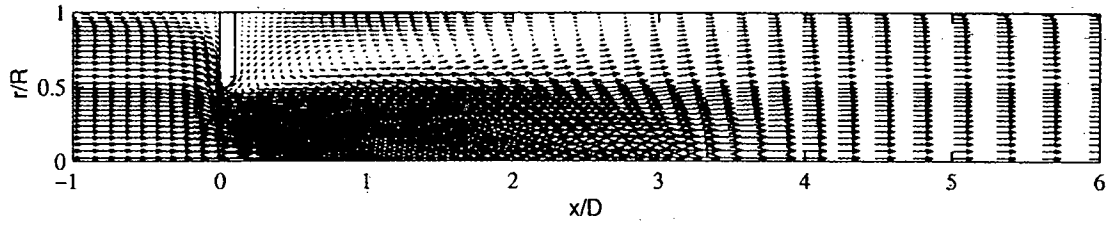

Fig. 7 Velocity vectors predicted by the SOU scheme

5. Concluding Remarks

Simulations of turbulent flow through a circular orifice plate have been carried out by utilizing the k-ε model and two different numerical schemes. The predicted results of mean flow properties were compared with measurements. The conclusions from the investigation can be drawn as follows:

1. The predicted centerline axial velocity and wall-static pressure profiles by the hybrid and SOU schemes are in generally good agreement with measurements.
2. The SOU shows a significant improvement over the hybrid scheme and both schemes give slightly over-predicted results in the core region and slightly under-predicted near the walls in comparison with measurements.

6. Acknowledgements

The authors would like to gratefully acknowledge the Thailand Research Fund for financial support of this research under contract no. PDF42/39.

7. References

1. Gatski, T.B. (1996), Turbulent Flows: Model Equations and Solution Methodology, in Handbook of Computational Fluid Mechanics, Edited by Roger Peyret, Academic Press Ltd, London.
2. Hogg, S. and Leschziner, M.A.(1989a), Computation of Highly Swirling Confined Flow with a Reynolds Stress Turbulence Model, AIAA J., Vol.27, pp.57-63.
3. Jones, W.P. and Pascau, A. (1989), Calculation of Confined Swirling Flows with a Second Moment Closure, Trans. ASME J. of Fluid Engineering, Vol.111, Sept, pp.248-255.
4. Nail, G.H. (1991), A Study of 3-dimensional flow through orifice meters, Ph.D. Dissertation, Texas A&M University.
5. Patankar, S.V. (1980), Numerical Heat Transfer and Fluid Flow, Hemisphere, Washington, D.C.
6. Patankar, S.V. and Spalding, D.B. (1970), Heat and Mass Transfer in Boundary Layers, Intertext Books, London.
7. Shyy, W., Thakur, S.,and Wright, J. (1992), Second Order Upwind and Central Difference Schemes for Recirculating Flow Computation, AIAA J., Vol.30, No.4, pp.931-932.
8. Sloan, D.G., Smith, P.J., and Smoot, L.D. (1986), Modeling of Swirl in Turbulent Flow System, Progr. Energy Combust. Sci., vol. 12, pp. 163-250.
9. Versteeg, H.K. and Malalasekera, W. (1995), An Introduction to Computational Fluid Dynamics: The Finite Volume Method, Longman Scientific & Technical, Longman Group Limited, Essex, England.
10. Wilcox, C.D. (1993), Turbulent Modelling for CFD, DCW Industries, Inc., California.